© 2014. Published by The Company of Biologists Ltd | Development (2014) 141, 2669-2679 doi:10.1242/dev.104331

RESEARCH ARTICLE

Larval mesenchyme cell specification in the primitive echinoid occurs independently of the double-negative gate

Atsuko Yamazaki[1,*], Yumi Kidachi[2], Masaaki Yamaguchi[3] and Takuya Minokawa[1]

ABSTRACT

Echinoids (sea urchins) are divided into two major groups – cidaroids (a 'primitive' group) and euechinoids (a 'derived' group). The cidaroids are a promising model species for understanding the ancestral developmental mechanisms in echinoids, but little is known about the molecular mechanisms of cidaroid development. In euechinoids, skeletogenic mesenchyme cell specification is regulated by the double-negative gate (DNG), in which hesC represses the transcription of the downstream mesenchyme specification genes (*alx1*, *tbr* and *ets1*), thereby defining the prospective mesenchyme region. To estimate the ancestral mechanism of larval mesenchyme cell specification in echinoids, the expression patterns and roles of mesenchyme specification genes in the cidaroid *Prionocidaris baculosa* were examined. The present study reveals that the expression pattern and function of hesC in *P. baculosa* were inconsistent with the DNG model, suggesting that the euechinoid-type DNG is not utilized during cidaroid mesenchyme specification. In contrast with hesC, the expression patterns and functions of alx1, tbr and ets1 were similar between *P. baculosa* and euechinoids. Based on these results, we propose that the roles of alx1, tbr and ets1 in mesenchyme specification were established in the common ancestor of echinoids, and that the DNG system was acquired in the euechinoid lineage after divergence from the cidaroid ancestor. The evolutionary timing of the establishment of the DNG suggests that the DNG was originally related to micromere and/or primary mesenchyme cell formation but not to skeletogenic cell differentiation.

KEY WORDS: Evolution, Mesoderm, Cidaroid, Sea urchin, Echinoderm, *Prionocidaris baculosa*

INTRODUCTION

Understanding how developmental mechanisms evolved is a predominant topic in the research of evolutionary biology, and echinoids (sea urchins) are an attractive model for this field. The embryonic development of indirectly developing regular sea urchins, such as *Strongylocentrotus purpuratus*, has been extensively examined, and knowledge of this gene regulatory network is accumulating (McClay, 2011). Additionally, various types of developmental modifications – e.g. putative ancestral developers and various derived modified developers, with developers being a species and/or group showing subjected developmental mode – are now recognized and are considered as potential subjects for evolutionary development studies (Schroeder, 1981; Wray and Raff, 1991). Based on both paleontological and molecular studies, a steadfast phylogenetic relationship that includes these various species has been hypothesized, and it provides a stable phylogenetic basis for evolutionary development studies (Smith, 1984; Kroh and Smith, 2010). Among echinoids, the cidaroid (a 'primitive' group of echinoids) has been considered as a crucial taxon to estimate the early evolutionary history (Schroeder, 1981; Wray and McClay, 1988). Because many characteristics of adult cidaroid morphology are considered to be ancestral, cidaroid development is also expected to preserve and reflect the ancestral state (Schroeder, 1981; Smith, 1984).

Although cidaroids have a pluteus larval stage that is similar to that of euechinoids (a 'derived' group of echinoids), their embryonic development clearly differs from that of euechinoids, particularly in relation to the process of mesoderm formation (Schroeder, 1981) (Fig. 1). Two types of mesenchyme cells are common in both euechinoids and cidaroids – skeletogenic cells and nonskeletogenic cells (Mortensen, 1921, 1938). The ontogeny of these two cell types in cidaroids, however, differs from that in euechinoids. In euechinoids, skeletogenic cells are derived from four micromeres at the vegetal pole of the 16-cell-stage embryo (Fig. 1E). The micromeres give rise to primary mesenchyme cells (PMCs), which ingress into the blastocoel before archenteron invagination and then differentiate into skeletogenic mesenchyme cells (Fig. 1F,H). During gastrulation, another type of mesenchyme cell emerges from the tip of the archenteron and differentiates into nonskeletogenic mesenchyme cells, such as pigment cells (Okazaki, 1975) (Fig. 1G,H). By contrast, in cidaroids, no typical micromere quartet is formed at the 16-cell stage (Schroeder, 1981; Yamazaki et al., 2012). Although the fourth cleavage in the vegetal hemisphere is unequal, the size of the blastomeres at the vegetal pole varies (Fig. 1A). The cidaroid embryos also have no typical PMCs (Fig. 1B). Both the skeletogenic and nonskeletogenic mesenchyme cells ingress after the initiation of archenteron invagination (Fig. 1C,D; supplementary material Fig. S2A2) (Schroeder, 1981; Emlet, 1988; Yamazaki et al., 2012).

The aforementioned differences in embryonic development strongly suggest that distinct molecular mechanisms are adopted for mesenchyme specification in cidaroids and euechinoids. In euechinoids, skeletogenic cell specification is regulated by the double-negative gate (DNG), a regulatory sub-circuit that consists of two sequential repressions by micro1 (also known as pmar1) and hesC (hairy/Enhancer of split C) (Revilla-i-Domingo et al., 2007). Micro1, a transcription repressor, is exclusively activated in the micromere quartet, and it blocks the transcription of *hesC*, another transcription repressor, in the micromeres. In the remaining part of the embryo, *hesC* is expressed and the product of this gene represses the transcription of downstream mesenchyme specification genes, including *alx1* (*aristaless-homeobox 1*), *tbr* (*T-brain*), *ets1* (*E26 transformation-specific 1*) and *delta*. The silencing of *hesC* by micro1 in the micromere lineages leads to specific activation of these mesenchyme specification genes (Kurokawa et al., 1999; Fuchikami et al., 2002; Kitamura et al., 2002; Oliveri et al., 2002; Sweet et al.,

[1]Research Center for Marine Biology, Graduate School of Life Sciences, Tohoku University, 9 Sakamoto, Asamushi, Aomori, Aomori 039-3501, Japan. [2]Department of Pharmacy, Faculty of Pharmaceutical Sciences, Aomori University, 2-3-1 Kobata, Aomori, Aomori 030-0943, Japan. [3]Division of Life Science, Graduate School of Natural Science and Technology, Kanazawa University, Kakuma, Kanazawa, Ishikawa 920-1192, Japan.

*Author for correspondence (yama0205@gmail.com)

Received 29 September 2013; Accepted 27 April 2014

Development (2014) 141, 2669-2679 doi:10.1242/dev.104331

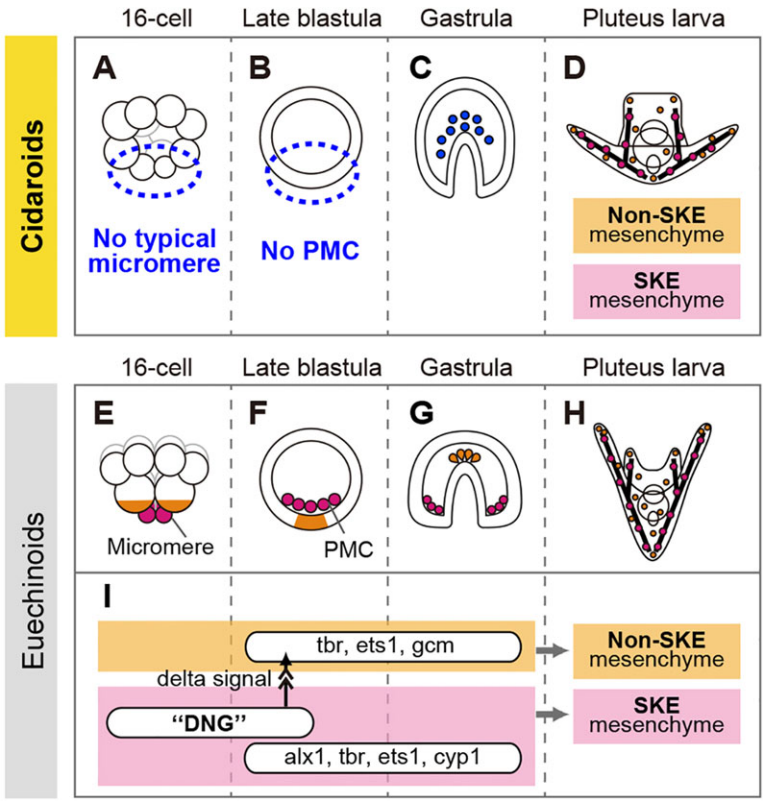

Fig. 1. The processes of mesenchyme formation in cidaroids and euechinoids. (A-D) Schematic diagram for the development of the cidaroid *P. baculosa*, which does not form the typical micromeres (A) or primary mesenchyme cells (PMCs) (B). The mesenchyme cells ingress from the tip of the archenteron, differentiating into both skeletogenic cells (SKE mesenchyme) and nonskeletogenic mesenchyme cells (Non-SKE mesenchyme; C,D). (E-H) Euechinoid development. At the 16-cell stage, four equally-sized micromeres are formed at the vegetal pole (E). The majority of micromere progenies give rise to PMCs (F) that eventually differentiate into larval skeletogenic cells (H). Non-SKE mesenchyme cells are derived from cells that have ingressed after the onset of gastrulation (G,H). Micromeres emit the non-SKE mesenchyme inductive signal (e.g. delta) to neighboring blastomeres. The molecular mechanism and genes that are responsible for this process have been well investigated (I). DNG: the double-negative gate.

2002; Ettensohn et al., 2003; Röttinger et al., 2004; Revilla-i-Domingo et al., 2007) (see Fig. 6B). The repression of transcription of *hesC* by micro1 is the core mechanism of DNG. Following DNG activation, the transcription of *cyp1* (*cyclophilin 1*) – which encodes a peptidylprolyl *cis-trans* isomerase and *gcm* (*glial cells missing*) – starts in skeletogenic and nonskeletogenic cells, respectively, which promotes the differentiation of each mesenchyme cell type (Fig. 1I; Amore and Davidson, 2006; Ransick and Davidson, 2006).

By contrast, the molecular mechanism of cidaroid development has scarcely been studied. The expression patterns of two putative endomesoderm specification genes in cidaroids – *wnt8* and *hox11/13b* – suggest that the molecular mechanism responsible for cidaroid endomesoderm formation is similar to that of euechinoids (Yamazaki et al., 2012); however, little is known about the expression patterns and functions of mesenchyme specification genes. Considering the fact that cidaroids have neither typical micromeres nor PMCs, it is probable that their mesenchyme cells are specified by a mechanism that differs from that of euechinoids.

In the present study, we isolated six genes – *hesC*, *alx1*, *tbr*, *ets1*, *gcm* and *cyp1* – from a cidaroid, *Prionocidaris baculosa*, and examined their expression patterns and functions in mesenchyme specification. Our results suggest that no euechinoid-type DNG exists in *P. baculosa*, although the roles of alx1, tbr, ets1 and gcm are similar between cidaroids and euechinoids.

RESULTS

Expression patterns of mesenchyme cell specification gene orthologs in *P. baculosa* embryos

Seven euechinoid genes that are involved in mesenchyme cell specification – *micro1*, *hesC*, *alx1*, *tbr*, *ets1*, *gcm* and *cyp1* – were selected and attempts were made to isolate the gene orthologs in *P. baculosa*. All orthologs, except for *micro1*, were successfully identified using degenerate polymerase chain reaction and rapid amplification of cDNA ends (RACE) PCR. Phylogenetic analyses based on the deduced amino acid sequences strongly support the orthology for the relevant genes (supplementary material Fig. S1). Therefore, we assigned the prefix Pb (*P. baculosa*) and designated these assembled cDNAs as *PbhesC* (Accession No. in the DNA Data Bank of Japan AB853323), *Pbalx1* (AB853324), *Pbtbr* (AB853325), *Pbets1* (AB853326), *Pbgcm* (AB853328) and *Pbcyp1* (AB853327).

The temporal and spatial expression profiles of these genes were analyzed by quantitative real-time PCR (qPCR) and whole-mount *in situ* hybridization (WMISH; Fig. 2 for late-blastula stage; Fig. 3 for late-gastrula stage; supplementary material Fig. S2 for other identified stages). At the late-blastula stage (16 h post-fertilization; hpf), *PbhesC* expression was observed in two regions – the vegetal pole (lower double-headed arrow in Fig. 2A,A″) and the presumptive ectodermal region (upper double-headed arrow in Fig. 2A). These two regions are separated by a torus domain that lacked expression of this gene (between the white arrowheads in Fig. 2A). The expression of *Pbalx1*, *Pbtbr*, *Pbets1* and *Pbgcm* was exclusively observed in the vegetal pole region (Fig. 2B-E,B″-E″). No localized expression of *Pbcyp1* was detected at the late-blastula stage (Fig. 2F). Thus, at this stage, all genes, except for *Pbcyp1*, were expressed together in the vegetal pole region. However, the widths of the expression domains were not identical (Fig. 2A′-E′). The proportions of the vegetal expression region of *PbhesC*, *Pbalx1*, *Pbtbr*, *Pbets1* and *Pbgcm* to the perimeter of the embryos (on average) were 12%, 8%, 11%, 15% and 11%, respectively. As summarized in Fig. 2G, the expression regions of *Pbalx1* and *Pbets1* were the narrowest and the broadest, respectively, whereas the sizes of the expression regions of *PbhesC*, *Pbtbr* and *Pbgcm* were intermediate to these.

In the late-gastrula stage (36 hpf), all genes were expressed in both mesenchyme cells (black arrowheads in Fig. 3A-F) and the

Development (2014) 141, 2669-2679 doi:10.1242/dev.104331

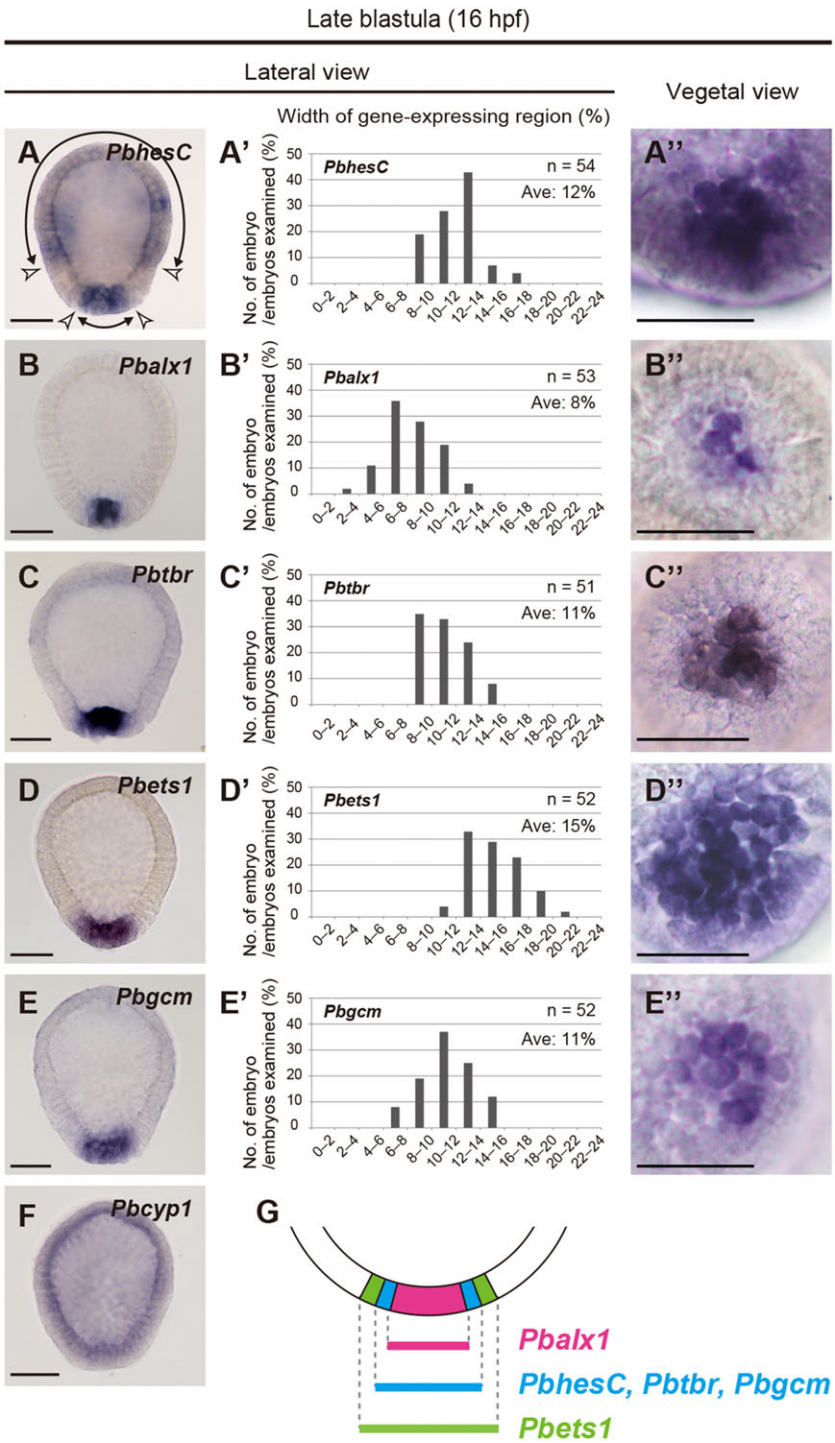

Fig. 2. The spatial expression of *PbhesC*, *Pbalx1*, *Pbtbr*, *Pbets1*, *Pbgcm* and *Pbcyp1* at the late-blastulae stage. The expression patterns of *PbhesC* (A), *Pbalx1* (B), *Pbtbr* (C), *Pbets1* (D), *Pbgcm* (E) and *Pbcyp1* (F) were analyzed at 16 h postfertilization (hpf) by using WMISH. (A-F) Lateral views. (A′-E′) Comparison of the width of the gene expression region at the vegetal pole when viewed laterally. The *x*-axis shows the proportion (%) of the expression region to the circumference of an embryo. The *y*-axis is the percentage of embryos divided into each width category. The total number of embryos analyzed (*n*) and the mean width of the expression regions (Ave) are shown in the upper right corner of each graph. (A″-E″) Vegetal views. (A) *PbhesC* expression is observed in two areas – a vegetal pole domain (lower double-headed arrow) and the presumptive ectoderm (upper double-headed arrow). (B-E) *Pbalx1*, *Pbtbr*, *Pbets1* and *Pbgcm* are expressed at the vegetal pole. (F) Localized expression of *Pbcyp1* is not detected. (G) A summarized drawing of the gene expression regions at the late-blastula stage. Of the five genes, the expression region of *Pbalx1* is the narrowest, whereas that of *Pbets1* is the broadest. Scale bars: 50 µm.

archenteron (brackets in Fig. 3A-F); however, the loci of expression were not identical. Two types of mesenchyme cells can be identified in the late gastrula – mesenchyme cells with skeletogenic cell-specific antigen (P4) expression (skeletogenic mesenchyme cells) (Shimizu et al., 1988) and those that lack P4 expression (nonskeletogenic mesenchyme cells). By simultaneously using WMISH and immunohistochemistry with P4 antibody, the gene expression patterns of the two mesenchyme cell types were revealed. *PbhesC* was expressed in both mesenchyme cell types (Fig. 3A′-A‴), whereas the expression of *Pbalx1* was observed in almost all skeletogenic cells but not in nonskeletogenic cells (Fig. 3B′-B‴). The expression of *Pbtbr* was observed in all skeletogenic cells and in some nonskeletogenic cells (Fig. 3C′-C‴); the expression of *Pbets1* and *Pbcyp1* was observed in almost all mesenchyme cells of both types (Fig. 3D′-D‴ and F′-F‴); and the expression of *Pbgcm* was observed in only a small portion of nonskeletogenic cells (Fig. 3E′-E‴). The expression patterns of these genes were classified into five patterns that are summarized in Fig. 3G.

The expression domains in the archenteron also differed among the genes (brackets in Fig. 3A-F). *PbhesC* expression was observed in the middle and lower region of the archenteron (Fig. 3A), whereas the rest of the genes were expressed in the tip of the archenteron or upper region (Fig. 3B-F). In addition, *PbhesC* and *Pbgcm* were expressed in parts of the ectodermal region (arrows in Fig. 3A,E).

Development (2014) 141, 2669-2679 doi:10.1242/dev.104331

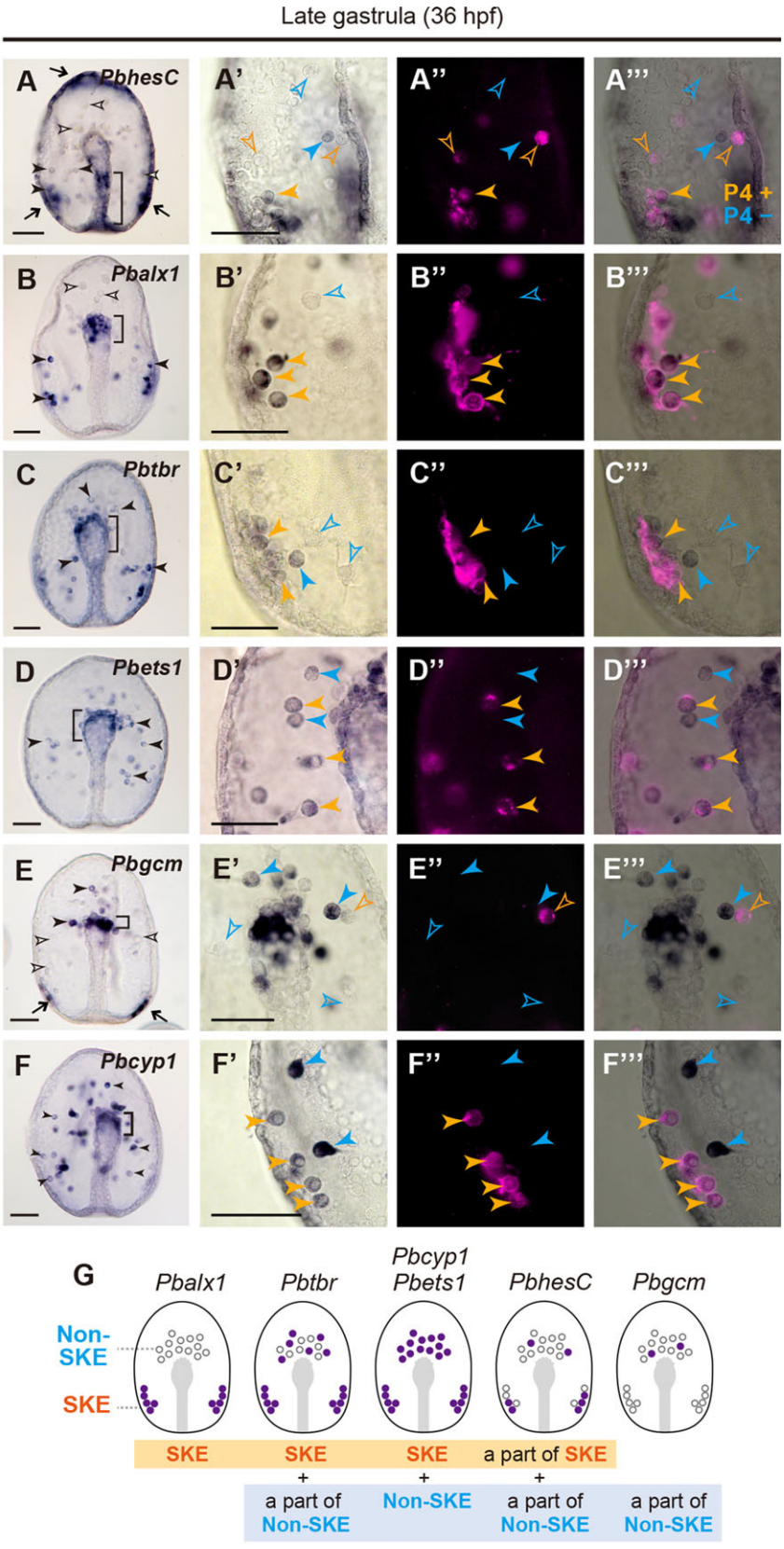

Fig. 3. The spatial expression patterns of *PbhesC*, *Pbalx1*, *Pbtbr*, *Pbets1*, *Pbgcm* and *Pbcyp1* at the late-gastrulae stage. The expression of *PbhesC* (A), *Pbalx1* (B), *Pbtbr* (C), *Pbets1* (D), *Pbgcm* (E) and *Pbcyp1* (F) at 36 hpf was examined. (A-F) Images of WMISH for the indicated genes. Black arrowhead, the mesenchyme cell expressing the indicated gene; white arrowhead, the mesenchyme cell without the gene expression; bracket, the gene expression domain in the archenteron. The expression of *PbhesC* and *Pbgcm* is also detected in the ectodermal region (arrows in A,E). (A′-F‴) Embryos analyzed by WMISH (bright field images; A′-F′) and immunohistochemistry using a skeletogenic cell-specific P4 antibody (fluorescent images; A″-F″). The merged images are shown in A‴-F‴. Orange arrowheads, P4-positive mesenchyme cells; blue arrowheads, P4-negative mesenchyme cells; solid arrowheads, mesenchyme cells expressing the subjected gene; open arrowheads, mesenchyme cells with no gene expression.
(G) Schematic diagram of the spatial gene expression patterns in mesenchyme cells. Purple dots represent cells expressing the indicated genes. Scale bars: 50 µm.

The absence of the euechinoid-type DNG in *P. baculosa* mesenchyme specification

The overlapping expression of *PbhesC* and mesenchyme specification genes at the vegetal pole of the blastula (Fig. 2G) suggests the absence of DNG in *P. baculosa* mesenchyme specification. To verify this possibility, we performed a perturbation experiment on PbhesC using morpholino antisense oligonucleotides (MOs) and examined the effects on the

Development (2014) 141, 2669-2679 doi:10.1242/dev.104331

expression of mesenchyme specification genes at the mid-blastula stage (12 hpf).

The perturbation of PbhesC did not affect the spatial expression patterns of all genes examined. There were no significant differences in the widths of gene expression domains between the control embryos that had been injected with an MO designed against *hesC* of another echinoid species, *Scaphechinus mirabilis* (*SmhesC*; hereafter, SmhesC-MO) and the experimental embryos (PbhesC-MO-injected embryos; hereafter, PbhesC-MO embryos) (Fig. 4Aa-Ea,Ab-Eb for images of embryos; Fig. 4Ac-Ed for the size distribution of the gene expression domains). This suggests that PbhesC does not participate in the spatial regulation of *Pbalx1*, *Pbtbr*, *Pbets1* and *Pbgcm*. The only visible difference between the control and PbhesC-MO embryos was the density of the WMISH signal for *PbhesC* (Fig. 4Ea,Eb).

The high intensity of the *PbhesC* WMISH signal in PbhesC-MO embryos suggested a repressive role for PbhesC on the transcription of *PbhesC* itself. To verify this possibility, qPCR analysis was conducted. The amount of transcribed *PbhesC* mRNA was significantly increased in the PbhesC-MO embryo (Fig. 4F), suggesting that PbhesC plays a repressive role in *PbhesC* transcription. The result of the increased *hesC* transcription in hesC-MO-injected embryos was also obtained when similar experiments were performed for two euechinoids, *S. mirabilis* and *Hemicentrotus pulcherrimus* (supplementary material Fig. S3B,C). These results strongly suggest that the

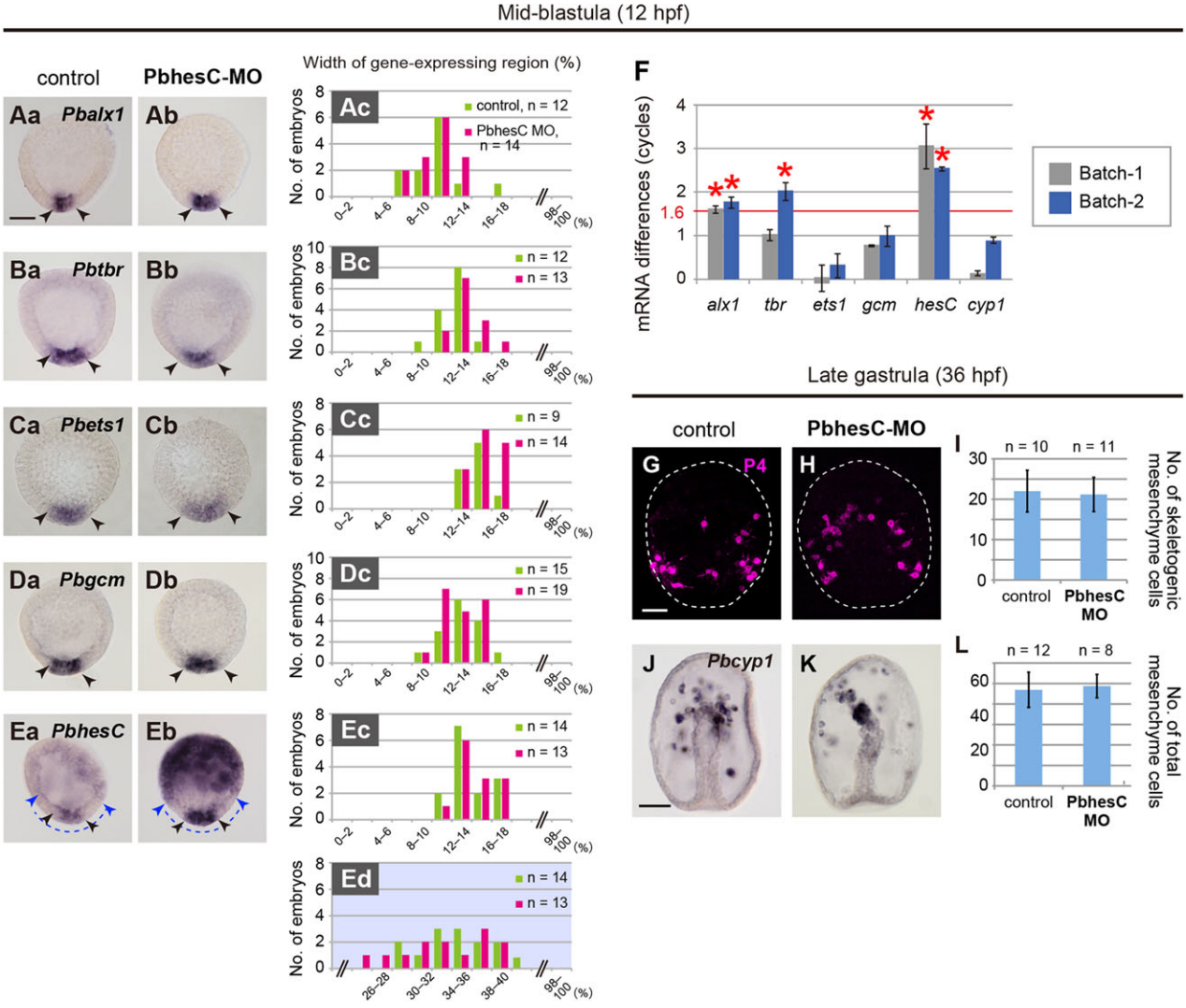

Fig. 4. Perturbation experiments of PbhesC. (A-E) WMISH analysis at the mid-blastula stage (12 hpf) of an embryo that had been injected with a morpholino antisense oligonucleotide (MO) against *PbhesC* (PbhesC-MO embryo). The expression of *Pbalx1* (Aa-Ac), *Pbtbr* (Ba-Bc), *Pbets1* (Ca-Cc), *Pbgcm* (Da-Dc) and *PbhesC* (Ea-Ed) was examined. (Aa-Ea) Control embryos were injected with an MO against *S. mirabilis hesC* (*SmhesC*). (Ab-Eb) PbhesC-MO embryos. (Ac-Ed) Measurement of the gene expression region widths. The width of the vegetal pole region between the black arrowheads in the left photograph was measured. For *PbhesC*, the Ed graph (shaded blue) shows the width of the vegetal expressing region plus a surrounding torus-like area that lacks expression (between blue arrowheads, a blue dashed line in Ea,Eb). In each graph, the number of embryos used for analysis in one batch is shown. PbhesC-MO does not affect the spatial expression patterns of any of the genes. (F) Quantitative real-time (qPCR) analysis in the PbhesC-MO embryo at the mid-blastula stage. The *y*-axis shows the qPCR cycle difference (Ct) when compared with that of the control. The results from two batches (gray and blue) are shown. Error bars represent the standard deviations. Red asterisks indicate an increase of 1.6 cycles or more. For *alx1* and *hesC*, both batches showed an increase in the transcript level above the standard. For *tbr*, the increase in the transcript level was detected only in one batch. (G-L) Measurement of the P4-expressing skeletogenic cell (G-I) and *Pbcyp1*-positive mesenchyme cell number (J-L) at the late-gastrula stage (36 hpf). (G,J) Control embryos. (H,K) PbhesC-MO embryos. The white dashed line in G and H shows the outline of the embryo. Each measurement result is shown in I and L. Error bars in the graphs show standard deviations. *n*=the number of embryos analyzed in the batch. PbhesC-MO does not affect the number of P4-expressing cells or *cyp1*-positive mesenchyme cells. Scale bars: 50 µm.

Development (2014) 141, 2669-2679 doi:10.1242/dev.104331

autorepression of *hesC* is a conserved function in echinoids. The specificity of the MOs was experimentally supported – no obvious change in the amount of *hesC* transcripts in all three species was observed when the hesC-MO that had been designed against a different species was introduced (supplementary material Fig. S3). These results indicate the efficacy and specificity of the PbhesC-MO in *P. baculosa* embryos, even though this MO did not alter the spatial expression patterns of *alx1*, *tbr* and *ets1*.

qPCR analyses also revealed the modest repressive potential of PbhesC on *Pbalx1* and *Pbtbr*. In PbhesC-MO embryos, an increase in the amount of *Pbalx1* transcript was detected in two batches (separate experiments using different eggs), and an increase in *Pbtbr* transcripts was detected in one of the two batches that were examined. No significant change was observed for the other three genes (*Pbcyp1*, *Pbets1* and *Pbgcm*; Fig. 4F).

To examine whether PbhesC plays a part in the differentiation of mesenchyme cells, PbhesC-MO embryos were reared to the late-gastrula stage, and the expression of the skeletogenic cell-specific P4 antigen and *Pbcyp1* (a pan-mesenchyme cell marker) was examined. No significant changes were observed in the number of either skeletogenic cells or total mesenchyme cells. The average numbers of P4-positive cells and *Pbcyp1*-expressing mesenchyme cells were approximately 20 and 55, respectively, in both control and PbhesC-MO embryos (Fig. 4G-L).

The roles of alx1, tbr and ets1 in mesenchyme cell differentiation in *P. baculosa*

Mesenchyme cell differentiation in euechinoids is regulated by various transcription factors – including alx1, tbr and ets1 (Kurokawa et al., 1999; Fuchikami et al., 2002; Ettensohn et al., 2003; Röttinger et al., 2004). The expression patterns of the *P. baculosa* orthologs resembled those in euechinoids (Figs 2 and 3), suggesting that these genes have similar roles to their counterparts in euechinoids. To examine the roles of these genes in the mesenchyme cell specification of *P. baculosa*, we performed functional perturbation experiments and examined the effects on mesenchyme cell differentiation. The functions of alx1 and tbr were perturbed by gene-specific MOs. To estimate the ets1 function, the MEK inhibitor U0126 was used because it blocks the mitogen-activated protein kinase (MAPK) pathway that is required for ets1 activation in euechinoids (Röttinger et al., 2004; Ettensohn et al., 2007).

First, we examined the effects on the differentiation of mesenchyme cells at the gastrula stage (36 hpf). The expression of *cyp1* was used as a pan-mesenchyme cell marker. The numbers of *cyp1*-positive mesenchyme cells in the Pbalx1-MO (Fig. 5B) and Pbtbr-MO embryos (Fig. 5C) were not significantly different from that in the control (control-MO embryo) (Fig. 5A) – the mean numbers were approximately 60 (Fig. 5E). By contrast, almost no migrating mesenchyme cells were observed in the U0126-treated embryos, and the number of *cyp1*-positive mesenchyme cells was strikingly decreased (approximately one cell per embryo upon treatment with U0126, and about 45 cells per embryo upon treatment with the control reagent dimethylsulfoxide) (Fig. 5D,E).

The differentiation of skeletogenic cells (Fig. 5F-I) and some of the nonskeletogenic mesenchyme cells (*Pbgcm*-positive cells) (Fig. 5K-N) at the late-gastrula stage was examined under perturbation. In the Pbalx1-MO and U0126-treated embryos, P4-positive skeletogenic cells were rarely formed (approximately one cell per embryo upon treatment with Pbalx1-MO, and less than one cell per embryo in those treated with U0126) (Fig. 5G,I,J). No significant difference in the number of P4-positive cells was observed between Pbtbr-MO and control-MO embryos (about 20 cells per embryo upon treatment with Pbtbr-MO, and 22 cells per embryo in control-MO embryos) (Fig. 5F,H,J).

The differentiation of *Pbgcm*-positive mesenchyme cells was strongly affected in Pbtbr-MO or U0126-treated embryos. In Pbtbr-MO embryos, the number of *Pbgcm*-positive mesenchyme cells (pink arrowheads) was approximately 60% or less than that in the control embryos (Fig. 5M,O). In U0126-treated embryos, there were almost no *gcm*-expressing mesenchyme cells; however, *Pbgcm* expression was observed in the tip of the archenteron and the bilateral ectodermal regions (Fig. 5N,O). Control and Pbalx1-MO embryos had a mean of 14-16 *gcm*-positive mesenchyme cells (pink arrowheads; Fig. 5K,L,O).

The larval skeletons and red-colored pigment cells are visible characteristics of mesenchyme differentiation in the pluteus larvae. To evaluate the effect on skeleton formation, the total length of postoral rods (TLPR, blue double-arrows in Fig. 5P-S) was measured. In the control pluteus larva (control-MO or dimethylsulfoxide-treated embryos), the TLPR was approximately 300-400 µm (Fig. 5P,T). The TLPR values in Pbalx1-MO, Pbtbr-MO and U0126-treated larvae were below 100 µm (Fig. 5Q-T). Pigment cell differentiation was severely affected by the perturbation of Pbtbr and Pbets1. Control pluteus larvae had 31-35 pigment cells on average (Fig. 5P,U). The number of pigment cells in Pbtbr-MO larvae was 19 on average, which is approximately 60% of the number of those in the control, whereas U0126-treated larvae had even fewer pigment cells (approximately five cells per embryo) (Fig. 5R,S,U). By contrast, in Pbalx1-MO larvae, the number of pigment cells was almost the same as that in the control (Fig. 5Q,U).

These effects caused by alx1-MO, tbr-MO and U0126 in *P. baculosa* were considerably similar to those observed previously in euechinoids (Fuchikami et al., 2002; Ettensohn et al., 2003; Röttinger et al., 2004). Based on these results, we suggest that alx1 is necessary for skeletogenic cell differentiation, that tbr is necessary for skeleton formation and pigment cell differentiation and that the MAPK pathway (and possibly ets1) is necessary for the general mesenchyme cell differentiation process and/or migration processes in *P. baculosa*. The reduction of *Pbgcm*-expressing mesenchyme cells and pigment cells in Pbtbr-MO embryos suggests that there is a role for Pbgcm in pigment cell differentiation.

DISCUSSION

The distinction of mesenchyme specification mechanisms between the cidaroids and euechinoids

The present study revealed various differences in the larval mesenchyme specification processes between the cidaroid *P. baculosa* and euechinoids. The most prominent question is as to whether DNG is involved in mesenchyme specification in cidaroids. In euechinoids, the complementary expression pattern of *hesC* with other component genes (*micro1*, *alx1*, *tbr* and *ets1*) is an indication of the existence of the DNG (Fig. 6B) (Revilla-i-Domingo et al., 2007). In *P. baculosa*, the overlapping expression patterns of *PbhesC* and mesenchyme specification genes in the vegetal pole region strongly suggest the absence of a euechinoid-type DNG that involves hesC (Fig. 2 and Fig. 6A), which is also supported by the PbhesC perturbation experiments (Fig. 4). Smith and Davidson (Smith and Davidson, 2009) have recently proposed the hypothesis that the DNG, consisting of hesC and blimp1, is an ancestral system in echinoids and that the micro1 initiation system might have developed more recently in the modern euechinoid lineage. However, the hesC-mediated DNG system, regardless of whether the repressor of *hesC* is micro1 or blimp1, seems to be

Development (2014) 141, 2669-2679 doi:10.1242/dev.104331

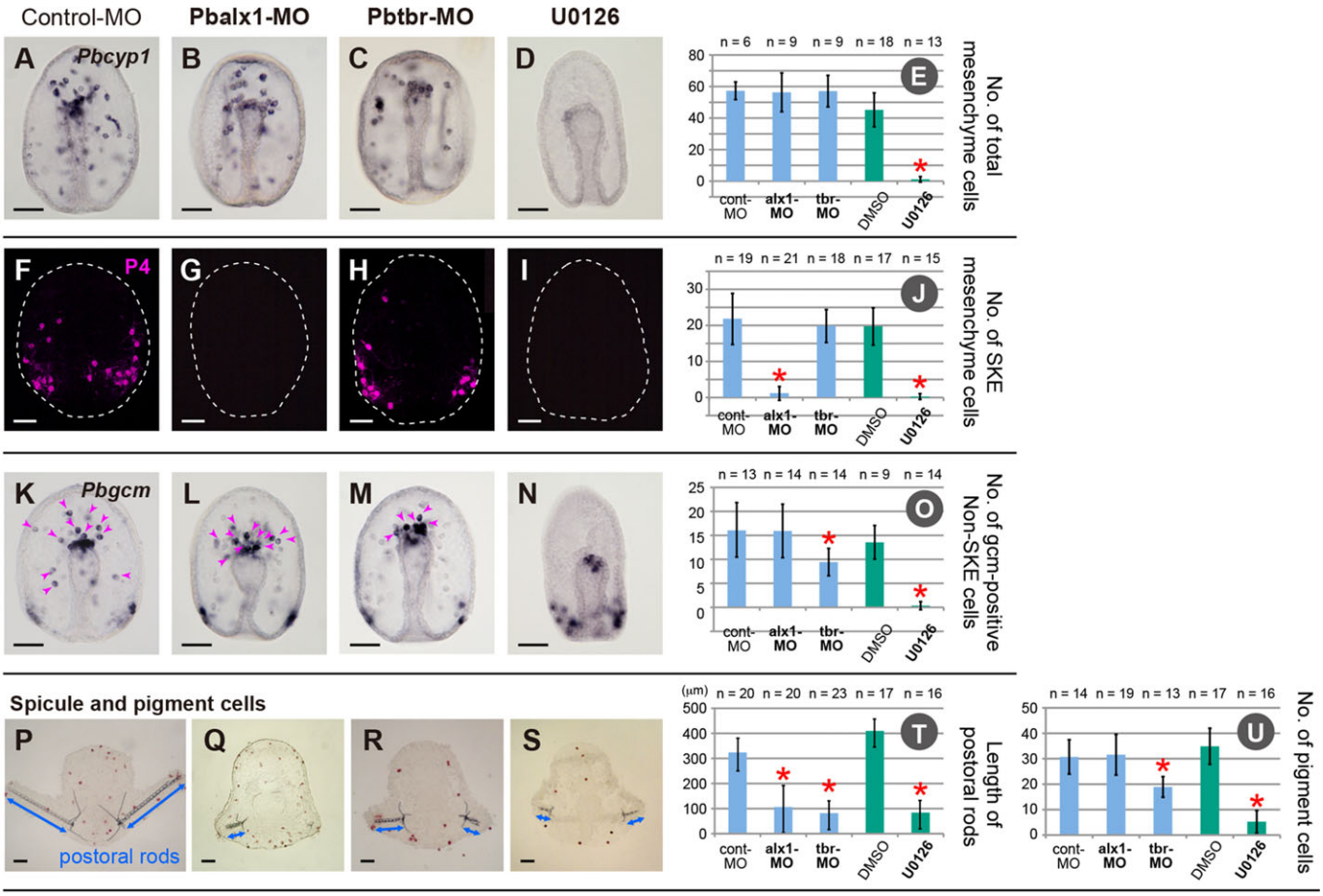

Fig. 5. Functional analysis of Pbalx1, Pbtbr and the MAPK pathway in skeletogenic and nonskeletogenic mesenchyme cell differentiation. Expression of alx1 and tbr was perturbed by using MOs, and U0126 was used to inhibit the MAPK pathway. (A-O) Visualization of *Pbcyp1*-expressing mesenchyme cells using WMISH (A-E), cells that expressed skeletogenic cell-specific P4 (F-J) and *Pbgcm*-positive nonskeletogenic mesenchyme cells using WMISH (pink arrowheads; K-O) at the late-gastrula stage (36 hpf). The white dashed line in F to I shows the outline of the embryo. (P-U) The measurement of the total length of bilateral postoral rods (blue double-headed arrows) and the number of pigment cells (red) at the pluteus larva stage (96 hpf). (A,F,K,P) Control embryos that had been injected with control-MO. (B,G,L,Q) Pbalx1-MO embryos. (C,H,M,R) Pbtbr-MO embryos. (D,I,N,S) Embryos treated with U0126. Scale bars: 50 μm. Each measurement result is shown in E, J, O, T and U. Error bars show the standard deviations. *n*=the number of embryos analyzed in each batch. Red asterisks indicate a significant difference between control and experimental embryos using the Mann–Whitney U test. Blue bars, results from experiments using MOs; green bars, results from experiments using reagents.

absent in the mesenchyme specification mechanism of cidaroids. The change from blimp1-mediated DNG to micro1-mediated DNG, if any, might have occurred in the euechinoid lineage after divergence from the cidaroid ancestor.

It might be postulated that *P. baculosa* contains a DNG framework that consists of an unknown repressor, instead of hesC, which controls the expression of *alx1*, *tbr* and *ets1*; however, this cannot be the case because the borders of the expression regions for *alx1*, *tbr* and *ets1* did not correspond with each other, even at the earliest stages, following the onset of their region-specific expression (Fig. 4A-C), suggesting that the spatial expression of these three genes is regulated through distinct factors rather than a single repressor.

Another difference is the timing of mesenchyme cell ingression (supplementary material Fig. S2A2). Unlike in the case of euechinoids, in all indirectly developing cidaroids that have been studied to date, mesenchyme cell ingression starts after the initiation of archenteron invagination (Schroeder, 1981; Emlet, 1988; present study). However, the order of the timing of the ingression of mesenchyme cell types can be similar to that in euechinoids – i.e. skeletogenic cells ingress early during development and pigment cells ingress later. In *P. baculosa*, the first ingressing mesenchyme cells at the mid-gastrula stage express both the skeletogenic cell-specific P4 antigen (supplementary material Fig. S2A2) and *Pbalx1* mRNA (supplementary material Fig. S2C2), suggesting that these cells are precursors of skeletogenic cells. A previous study on another cidaroid, *Eucidaris tribuloides*, has also demonstrated that the skeletogenic cells ingress at an earlier stage (Wray and McClay, 1988). The ingression of nonskeletogenic mesenchyme cells follows the ingression of skeletogenic cells. Our study shows that *Pbgcm*-expressing mesenchyme cells, which are possibly pigment cell precursors, ingress long after the appearance of skeletogenic cells (Fig. 3E; supplementary material Fig. S2F2). The order of the ingression of skeletogenic cells, which is followed by that of pigment cells, seems to have been established in the echinoid ancestor.

The existence of DNG is not the only feature that distinguishes euechinoids from cidaroids on a molecular level. The present results suggest that the array of genes involved in skeletogenic cell differentiation had been also modified during echinoid evolution. In the euechinoid *S. purpuratus*, *cyp1* is specifically expressed in the skeletogenic mesenchyme region (Amore and Davidson, 2006). Alternatively, in *P. baculosa*, almost all mesenchyme cells expressed *cyp1* (Fig. 3F), suggesting that cyp1 is involved in the differentiation

Development (2014) 141, 2669-2679 doi:10.1242/dev.104331

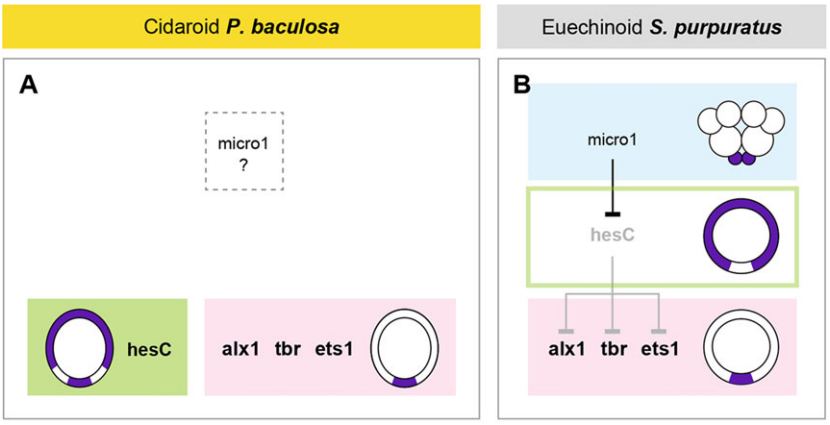

Fig. 6. Schematic diagrams of gene expression patterns and gene regulation at the blastula stage of *P. baculosa* and *S. purpuratus*. The genes expressed at the vegetal pole are shown in black characters, whereas the gene indicated in gray (hesC in *S. purpuratus*) is not expressed at the vegetal pole. In the diagrams, only the repressive inputs that turn off the downstream genes are shown. (A) The results of our perturbation experiments and the overlapping expression of *PbhesC* and the other mesenchyme specification genes do not support the DNG model in *P. baculosa*. PbhesC does not affect the spatial regulations of *alx1*, *tbr* and *ets1*, although PbhesC quantitatively represses the transcription of itself and *alx1* (plus potentially *tbr*). We could not isolate the *micro1* (*pmar1*) ortholog from this species. In the model of *S. purpuratus* (B), the DNG, comprising micro1 and hesC, plays an important role for spatial regulation of the mesenchyme specification genes *alx1*, *tbr* and *ets1*. *micro1* is specifically activated at the micromere of the 16-cell stage, resulting in transcriptional repression of hesC, which represses *alx1*, *tbr* and *ets1*. Thus, the expression of *alx1*, *tbr* and *ets1* takes place in the micromere region at the blastula stage (Revilla-i-Domingo et al., 2007).

of all mesenchyme cell types. The PMC-restricted expression pattern of *cyp1* in *S. purpuratus* strongly suggests that an evolutionary modification occurred of cyp1 function in the euechinoid lineage.

Evolution of the molecular mechanism for larval mesenchyme specification

For more than three decades, it has been deemed that the developmental mechanism for mesenchyme specification was modified in modern euechinoids during echinoid evolution (Schroeder, 1981). However, it is still unknown how a molecular mechanism effected this change. In the present study, we hypothesize that the introduction of the DNG is one of the crucial modifications in the euechinoid ancestor. Based on the study of asteroid embryos, McCauley and colleagues (McCauley et al., 2010) have suggested that the DNG is a novelty of euechinoids. The result of the present study supports this view of McCauley et al. and provides experimental evidence to suggest that there is an absence of the DNG in the ancestral mechanism of echinoids.

Our study shows that there are two types of molecular mechanism that specify the mesenchyme in echinoids – i.e. the mechanism without DNG, which is observed in *P. baculosa*, and that with DNG, which is observed in euechinoids. These findings could indicate one of the two following evolutionary scenarios – first, *P. baculosa* retained its ancestral mechanism and DNG evolved in the lineage of euechinoids; second, the echinoid ancestor had already obtained DNG and cidaroids lost DNG following divergence from the euechinoid lineage. We consider the former possibility to be more likely because it has also been suggested that another group of echinoderms – the asteroid group – does not use DNG. In the asteroid embryos, *hesC*, *alx1*, *tbr* and *ets1* are co-expressed at the vegetal pole of the blastula (Fig. 7) and perturbation of hesC does not affect the spatial expression of *tbr* and *ets1* (McCauley et al., 2010, 2012). The similarity between the asteroid and cidaroid leads us to conclude that the mesenchyme specification mechanism without DNG is the ancestral trait of echinoids.

We further propose that DNG was established in the common ancestor of euechinoids (asterisk in the phylogenetic tree of Fig. 7). We have previously shown that the DNG-characteristic gene expression pattern is also observed in the euechinoid *S. mirabilis*, the ancestor of which had been separated from the camarodonta (the group including *S. purpuratus*) approximately 200 million years ago (Yamazaki et al., 2010) (Fig. 7), indicating that the euechinoid ancestor had obtained DNG.

This study on cidaroids might also provide the key towards understanding the evolutionary history of echinoderms. Our data suggest that the functions of alx1, tbr, ets1 and gcm had been established before the diversification of echinoids, because the roles of these genes are quite similar between *P. baculosa* and euechinoids (Fig. 5) (Kurokawa et al., 1999; Fuchikami et al., 2002; Ettensohn et al., 2003; Röttinger et al., 2004; Ransick and Davidson, 2006). Tbr might have been recruited for the specification of both skeletogenic and pigment cells, whereas gcm might have been recruited for the specification of pigment cells in the common ancestor of echinoids (see circle in the phylogenetic tree in Fig. 7). It is likely that, in echinoderm embryos, tbr and gcm lack these functions. The asteroids do not form larval skeletons and pigment cells, whereas holothuroid embryos have no pigment cells (Ben-Tabou de-Leon and Davidson, 2009; Takata and Kominami, 2011; McCauley et al., 2012). In addition, holothuroid tbr is not responsible for skeletogenic cell specification (McCauley et al., 2012). Our data also support previous notions about the origins of alx1 and ets1 functions – that these were obtained before diversification of the echinoid from holothuroids, a closely related echinoderm class (square and triangle in the phylogenetic tree in Fig. 7) (McCauley et al., 2012; Koga et al., 2010).

The relevance of DNG to micromere and PMC formation

The present study provides a new interpretation of DNG function. To date, DNG has been considered to be a starting point in the series that leads to the specification of skeletogenic cells (from the micromere to PMC to larval skeletogenic cell lineage) (Revilla-i-Domingo et al., 2007; Li and Davidson, 2009). However, the larval skeletogenesis in the absence of DNG in *P. baculosa* indicates that this regulatory subcircuit is not essential for larval skeletogenesis. Two previous studies in euechinoids also support this idea – first, the knockdown of *micro1* prevents PMC ingression but not skeletogenesis (Smith and

Development (2014) 141, 2669-2679 doi:10.1242/dev.104331

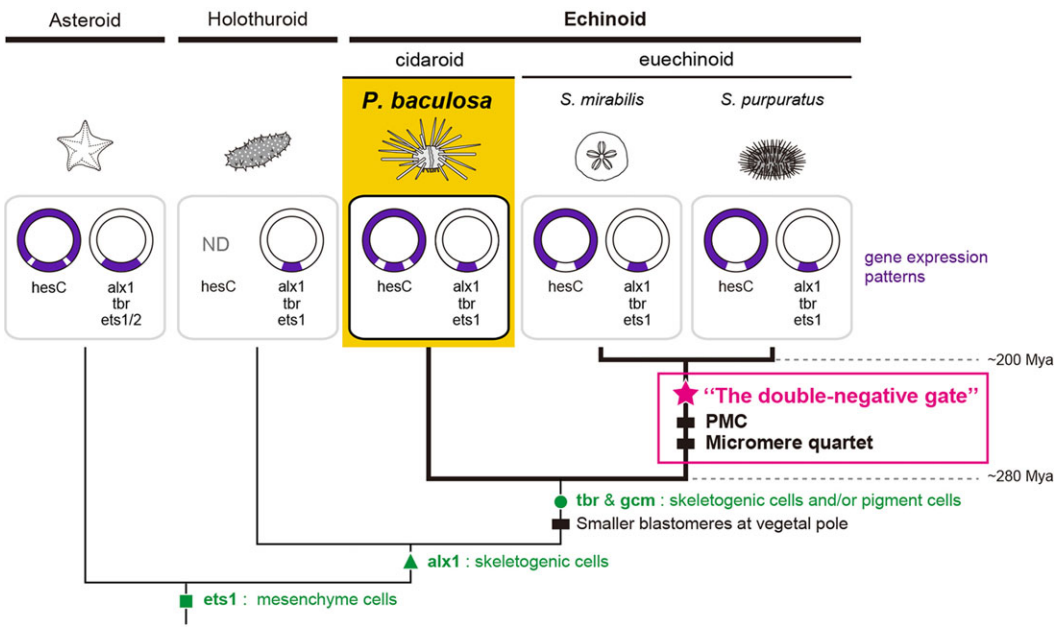

Fig. 7. A hypothetical evolutionary history of the larval mesenchyme specification mechanism in echinoderm. The diagram shows the relationships between three echinoids (two euechinoids *S. mirabilis* and *S. purpuratus* and the cidaroid *P. baculosa*), a holothuroid and an asteroid, as well as gene expression patterns at the blastula stage of each embryo. The classification and divergence time of the taxa and the information regarding gene expression have been taken from previous studies (Smith et al., 2004; Revilla-i-Domingo et al., 2007; Kroh and Smith, 2010; McCauley et al., 2010, 2012; Yamazaki et al., 2010). The expression profile of holothuroid *hesC* has not been described (ND). Green and pink marks on the phylogenetic tree indicate the acquisition of the character at the molecular level, and black boxes represent the introduction of a new characteristic on the cellular and morphological levels. The acquisitions of *alx1*, *tbr*, *ets1* and *gcm* functions took place in, or before, the echinoid ancestor (green marks) because these functions are common in the cidaroid and euechinoid. However, the double-negative gate (DNG), including hesC, was acquired – along with the micromere quartet and PMC – in the euechinoid ancestor (pink box) because there is no DNG in the cidaroid or asteroid.

Davidson, 2009), and second, ectopic activation of *micro1* is not required for the regulation of skeletogenic cell formation in a non-PMC region, which occurs by removing PMCs (Ettensohn et al., 2007). However, it is noteworthy that DNG and micromeres and/or PMCs seem to have been synchronously acquired in the common ancestor of euechinoids (pink box in the phylogenetic tree of Fig. 7) (Gao and Davidson, 2008; Yamazaki et al., 2012; present study). Therefore, we now assume that the acquisition of DNG in the euechinoid ancestor is associated with micromere- and/or PMC-related evolutionary events – e.g. the fine-tuning of unequal cleavage mechanisms to produce a typical micromere quartet, and/or a heterochronic shift in the onset of mesenchyme ingression to occur earlier than the onset of gastrulation.

MATERIALS AND METHODS

Animals and embryos

The collection of adult *P. baculosa*, *S. mirabilis* and *H. pulcherrimus*, and the handling of gametes and embryos were performed according to a previously described method (Yamazaki et al., 2010, 2012). To estimate the transition of total cell numbers during the early stages of development in *P. baculosa* embryos, the number of nuclei per embryo were counted after staining with propidium iodide (Nacalai Tesque), as described previously (Stickland et al., 2004) (supplementary material Table S1).

Isolation of genes from *P. baculosa*

A conventional degenerate PCR method was used to isolate the partial sequence of *hesC*, *alx1*, *tbr*, *ets1*, *gcm* and *cyp1* from *P. baculosa*. For cloning of *tbr* and *ets1*, primer sets that have been described previously were used (Koga et al., 2010; Minemura et al., 2009). For the remaining the genes, the primers listed in supplementary material Table S2 were used. To isolate 5′ and 3′ fragments, RACE was performed using primers shown in supplementary material Table S2. The template cDNA synthesis and PCR amplification were performed as described previously (Yamazaki et al., 2012). We obtained full-length sequences for *hesC*, *alx1* and *tbr* and 3′ partial sequences for *ets1*, *gcm* and *cyp1*.

qPCR

qPCR analysis was performed as described previously (Yamazaki et al., 2012). The primer sequences used are described in supplementary material Table S2. The *mitochondrial cytochrome c oxidase subunit 1* gene (*mitCO1*) was used for the internal reference standard. The sequence of the *mitCO1* gene from *S. mirabilis* (*SmmitCO1*) has been deposited in the DNA Data Bank of Japan with the accession number AB900169. For the hesC perturbation experiments, a difference of 1.6 or more in the Ct value between perturbed and control embryos was considered significant, as described previously (Oliveri and Davidson, 2004).

Whole-mount *in situ* hybridization

WMISH was performed as described previously (Yamazaki et al., 2012). For hybridization, we used a mixture of two probes that had been derived from 5′ and 3′ RACE fragments of *PbhesC*, *Pbalx1* or *Pbtbr* and the probe from 3′ RACE fragments of *Pbets1*, *Pbgcm* or *Pbcyp1*. When WMISH, using sense probes, was performed, staining at a level higher than the background was not observed for any genes.

Measurement of gene expression regions at the blastula stage

The lateral view photographs of the blastulae that had been stained by using WMISH were taken and analyzed by using Illustrator CS5 (Adobe Systems). A circular template was prepared and transformed to fit the perimeter of the embryo. We then measured both the length of the arc in the region where the gene of interest was expressed and that of the outer circumference of the embryo and then calculated the percentage of the arc that was within the circumference. Embryos were classified into categories that were divided every 2%, i.e. '2% and more' and 'under 4%', according to the percentage of

Development (2014) 141, 2669-2679 doi:10.1242/dev.104331

the expression region. The proportion of each expression sector relative to the perimeter was measured in more than 50 embryos for each gene.

Evaluation of mesenchyme cell differentiation

Skeletogenic cell differentiation was evaluated using the P4 antibody, which recognizes the skeletogenic cell-specific glycoprotein in *H. pulcherrimus* (Shimizu et al., 1988). The embryos that had been fixed for WMISH analysis, or the embryos that had been stained using WMISH, were washed with MOPS buffer three times and then incubated in MOPS buffer containing the P4 antibody (diluted 1:500) for 1 h at room temperature. After being rinsed five times, the embryos were incubated with the secondary goat antibody against mouse IgGs (heavy and light chains) Hilyte Fluor 555-Labeled (diluted 1:200; AnaSpec) for 1 h at room temperature. The embryos were further washed with MOPS buffer five times and then transferred to 50% glycerol for observation. The embryos were examined by using an epifluorescence inverted microscope (Leica DM IL).

To evaluate the larval skeleton formation, the TLPR value was used. TLPR was calculated as the sum of the length of bilateral fenetrated postoral rods (blue double arrows in Fig. 5P-S). The number of pigment cells was counted, as previously described (Kominami, 1998), using a Nikon Optiphot microscope.

Perturbation experiments

The translational perturbations were performed using MOs (GeneTool). Sequence-specific MOs were synthesized against *PbhesC*, *Pbalx1*, *Pbtbr*, *SmhesC* and *HphesC*. The MO sequences were as follows: PbhesC-MO, 5′-CACAAAGATCTGCTGATGAAATCAT-3′; Pbalx1-MO, 5′-ACGGC-ATGGAGCGGTAGAAAATCAT-3′; Pbtbr-MO, 5′-TCGCTTCAAAAT-CCTCACTCATCAT-3′; and SmhesC-MO, 5′-AGTTAGTACAAGTGG-TAGTCATCAT-3′. For the perturbation of HphesC, we used an MO that has been described previously (Ochiai et al., 2010).

The MOs were introduced into the embryos by using microinjection. After fertilization in filtered natural seawater, the jelly layer was removed by treatment with acidic seawater containing 1 mM sodium citrate. The fertilized eggs were placed on the bottom of protamine-coated dishes that had been filled with seawater containing 1 mM 3-amino 1,2,4-triazole (ATA). For *H. pulcherrimus*, fertilization was performed just before microinjection. MOs were diluted with 0.2 M KCl to 1 mM. For experiments on *S. mirabilis*, 0.25 mM MO solutions were used. The injection volume was approximately 1/64 of the quantity of the egg volume (the final concentration was approximately 15 µM when using a 1 mM MO solution). In experiments on *P. baculosa*, we also attempted to inject 0.25 mM MO solutions and obtained similar effects – e.g. an increase of *hesC* mRNA and inhibition of skeleton formation in the case of PbhesC-MO and Pbalx1-MO, respectively. By contrast, the lower concentration of Pbtbr-MO caused no effect. Microinjection into fertilized eggs was performed until 50 min, 40 min and 60 min after fertilization for *P. baculosa*, *S. mirabilis* and *H. pulcherrimus*, respectively.

The MEK inhibitor U0126 was used to inhibit the MAPK pathway that is essential for ets1 activation in euechinoids (Röttinger et al., 2004). Embryos were treated with 5 µM U0126 (Merck) in seawater from 2 hpf until 36 hpf. We also attempted treatment with 25 µM or 1 µM U0126. Treatment with 25 µM U0126 caused embryonic lethality or a defect in hatching, whereas 1 µM U0126-treated embryos had a small number of mesenchyme cells at the late-gastrula stage. As a control, 1 µl/ml DMSO in seawater was used. Experimental embryos were cultured in seawater containing penicillin G potassium (100 unit/ml) and streptomycin sulfate (50 µg/ml). During the culture, the seawater was changed daily. All the experiments were conducted in more than two batches.

Acknowledgements

We thank Masashi Noguchi, Setsuo Kiyomoto, Norihiko Deguchi, Toshimitsu Fukuhata and Katsuhiko Furukawa for the collection of the adult *P. baculosa*. We also thank Takaharu Numakunai for the *P. baculosa* culture system; Ryoichi Matsuda and Hideki Katow for providing the P4 antibody; and Shunsuke Yaguchi for the support in a part of gene expression analyses. qPCR analyses were performed in the core facility for research equipment at Aomori University.

Competing interests

The authors declare no competing financial interests.

Author contributions

A.Y. and T.M. designed the research, analyzed data and wrote the paper. A.Y. undertook experiments. Y.K. helped with qPCR analysis. M.Y. helped in the collection of total RNA from *P. baculosa* and provided comments on the design of the research and manuscript.

Funding

This study was supported by a Grant-in-Aid for Japan Society for the Promotion of Science Fellows [10J04441 to A.Y.] and a Grant-in-Aid for Scientific Research [C: 22570198 to T.M.] from the Japan Society for the Promotion of Science.

Supplementary material

Supplementary material available online at
http://dev.biologists.org/lookup/suppl/doi:10.1242/dev.104331/-/DC1

References

Amore, G. and Davidson, E. H. (2006). cis-Regulatory control of cyclophilin, a member of the ETS-DRI skeletogenic gene battery in the sea urchin embryo. *Dev. Biol.* **293**, 555-564.

Ben-Tabou de-Leon, S. and Davidson, E. H. (2009). Experimentally based sea urchin gene regulatory network and the causal explanation of developmental phenomenology. *Wiley Interdiscip. Rev. Syst. Biol. Med.* **1**, 237-246.

Emlet, R. B. (1988). Larval form and metamorphosis of a “primitive” sea urchin, *Eucidaris thouarsi* (Echinodermata: Echinoidea: Cidaroida), with implications for developmental and phylogenetic studies. *Biol. Bull.* **174**, 4-19.

Ettensohn, C. A., Illies, M. R., Oliveri, P. and De Jong, D. L. (2003). Alx1, a member of the Cart1/Alx3/Alx4 subfamily of Paired-class homeodomain proteins, is an essential component of the gene network controlling skeletogenic fate specification in the sea urchin embryo. *Development* **130**, 2917-2928.

Ettensohn, C. A., Kitazawa, C., Cheers, M. S., Leonard, J. D. and Sharma, T. (2007). Gene regulatory networks and developmental plasticity in the early sea urchin embryo: alternative deployment of the skeletogenic gene regulatory network. *Development* **134**, 3077-3087.

Fuchikami, T., Mitsunaga-Nakatsubo, K., Amemiya, S., Hosomi, T., Watanabe, T., Kurokawa, D., Kataoka, M., Harada, Y., Satoh, N., Kusunoki, S. et al. (2002). T-brain homologue (HpTb) is involved in the archenteron induction signals of micromere descendant cells in the sea urchin embryo. *Development* **129**, 5205-5216.

Gao, F. and Davidson, E. H. (2008). Transfer of a large gene regulatory apparatus to a new developmental address in echinoid evolution. *Proc. Natl. Acad. Sci. U.S.A.* **105**, 6091-6096.

Kitamura, K., Nishimura, Y., Kubotera, N., Higuchi, Y. and Yamaguchi, M. (2002). Transient activation of the *micro1* homeobox gene family in the sea urchin (*Hemicentrotus pulcherrimus*) micromere. *Dev. Genes Evol.* **212**, 1-10.

Koga, H., Matsubara, M., Fujitani, H., Miyamoto, N., Komatsu, M., Kiyomoto, M., Akasaka, K. and Wada, H. (2010). Functional evolution of Ets in echinoderms with focus on the evolution of echinoderm larval skeletons. *Dev. Genes Evol.* **220**, 107-115.

Kominami, T. (1998). Role of cell adhesion in the specification of pigment cell lineage in embryos of the sea urchin, *Hemicentrotus pulcherrimus*. *Dev. Growth Differ.* **40**, 609-618.

Kroh, A. and Smith, A. B. (2010). The phylogeny and classification of post-Palaeozoic echinoids. *J. Syst. Palaeontol.* **8**, 147-212.

Kurokawa, D., Kitajima, T., Mitsunaga-Nakatsubo, K., Amemiya, S., Shimada, H. and Akasaka, K. (1999). HpEts, an ets-related transcription factor implicated in primary mesenchyme cell differentiation in the sea urchin embryo. *Mech. Dev.* **80**, 41-52.

Li, E. and Davidson, E. H. (2009). Building developmental gene regulatory networks. *Birth Defects Res. C Embryo Today* **87**, 123-130.

McCauley, B. S., Weideman, E. P. and Hinman, V. F. (2010). A conserved gene regulatory network subcircuit drives different developmental fates in the vegetal pole of highly divergent echinoderm embryos. *Dev. Biol.* **340**, 200-208.

McCauley, B. S., Wright, E. P., Exner, C., Kitazawa, C. and Hinman, V. F. (2012). Development of an embryonic skeletogenic mesenchyme lineage in a sea cucumber reveals the trajectory of change for the evolution of novel structures in echinoderms. *EvoDevo* **3**, 17.

McClay, D. (2011). Evolutionary crossroads in developmental biology: sea urchins. *Development* **138**, 2639-2648.

Minemura, K., Yamaguchi, M. and Minokawa, T. (2009). Evolutionary modification of T-brain (tbr) expression patterns in sand dollar. *Gene Expr. Patterns* **9**, 468-474.

Mortensen, T. H. (1921). *Studies of the Development and Larval Forms of Echinoderms*. Copenhagen: G E C GAD.

Mortensen, T. H. (1938). Contributions to the study of the development and larval forms of echinoderms IV. *Kgl. Dan. Vidensk. Selsk., Skr. Naturvid. Math. Ser. 9* **7**, 1-59.

Ochiai, H., Fujita, K., Suzuki, K., Nishikawa, M., Shibata, T., Sakamoto, N. and Yamamoto, T. (2010). Targeted mutagenesis in the sea urchin embryo using zinc-finger nucleases. *Genes Cells* **15**, 875-885.
Okazaki, K. (1975). Biochemistry and morphogenesis. In *The Sea Urchin Embryo* (ed. G. Czihak), pp. 177-232. Heidelberg: Springer-Verlag.
Oliveri, P. and Davidson, E. H. (2004). Gene regulatory network analysis in sea urchin embryos. *Methods Cell Biol.* **74**, 775-794.
Oliveri, P., Carrick, D. M. and Davidson, E. H. (2002). A regulatory gene network that directs micromere specification in the sea urchin embryo. *Dev. Biol.* **246**, 209-228.
Ransick, A. and Davidson, E. H. (2006). cis-regulatory processing of Notch signaling input to the sea urchin glial cells missing gene during mesoderm specification. *Dev. Biol.* **297**, 587-602.
Revilla-i-Domingo, R., Oliveri, P. and Davidson, E. H. (2007). A missing link in the sea urchin embryo gene regulatory network: hesC and the double-negative specification of micromeres. *Proc. Natl. Acad. Sci. U.S.A.* **104**, 12383-12388.
Röttinger, E., Besnardeau, L. and Lepage, T. (2004). A Raf/MEK/ERK signaling pathway is required for development of the sea urchin embryo micromere lineage through phosphorylation of the transcription factor Ets. *Development* **131**, 1075-1087.
Schroeder, T. E. (1981). Development of a “primitive” sea urchin (*Eucidaris tribuloides*): irregularities in the hyaline layer, micromeres, and primary mesenchyme. *Biol. Bull.* **161**, 141-151.
Shimizu, K., Noro, N. and Matsuda, R. (1988). Micromere differentiation in the sea urchin embryo: expression of primary mesenchyme cell specific antigen during development. (sea urchin/micromere/primary mesenchyme cell/monoclonal antibody). *Dev. Growth Differ.* **30**, 35-47.
Smith, A. (1984). *Echinoid Palaeobiology*. London: George Allen & Unwin.
Smith, J. and Davidson, E. H. (2009). Regulative recovery in the sea urchin embryo and the stabilizing role of fail-safe gene network wiring. *Proc. Natl. Acad. Sci. U.S.A.* **106**, 18291-18296.
Smith, A. B., Peterson, K. J., Wray, G. and Littlewood, D. T. J. (2004). From bilateral symmetry to pentaradiality: the phylogeny of hemichordates and echinoderms. In *Assembling the Tree of Life* (ed. J. Cracraft and M. J. Donoghue), pp. 365-383. New York: Oxford University Press.
Stickland, L., von Dassow, G., Ellenberg, J., Foe, V., Lenart, P. and Burgess, D. (2004). Light microscopy of echinoderm embryos. *Methods Cell Biol.* **74**, 371-409.
Sweet, H. C., Gehring, M. and Ettensohn, C. A. (2002). LvDelta is a mesoderm-inducing signal in the sea urchin embryo and can endow blastomeres with organizer-like properties. *Development* **129**, 1945-1955.
Takata, H. and Kominami, T. (2011). Novel population of embryonic secondary mesenchyme cells in the keyhole sand dollar *Astriclypeus manni*. *Dev. Growth Differ.* **53**, 625-638.
Wray, G. and McClay, D. R. (1988). The origin of spicule-forming cells in a ‘primitive’ sea urchin (Eucidaris tribuloides) which appears to lack primary mesenchyme cells. *Development* **103**, 305-315.
Wray, G. A. and Raff, R. A. (1991). The evolution of developmental strategy in marine invertebrates. *Trends Ecol. Evol.* **6**, 45-50.
Yamazaki, A., Furuzawa, Y. and Yamaguchi, M. (2010). Conserved early expression patterns of micromere specification genes in two echinoid species belonging to the orders clypeasteroida and echinoida. *Dev. Dyn.* **239**, 3391-3403.
Yamazaki, A., Kidachi, Y. and Minokawa, T. (2012). “Micromere” formation and expression of endomesoderm regulatory genes during embryogenesis of the primitive echinoid *Prionocidaris baculosa*. *Dev. Growth Differ.* **54**, 566-578.

Supporting Information Figure Legends

Fig. S1.

The identification of genes isolated from *Prionocidaris baculosa*. Alignments of deduced amino acid sequences and construction of phylogenetic trees were performed using MacClade 4.08 (http://macclade.org/macclade.html) and Clustal X (http://www.clustal.org/clustal2/) on the sequences listed below: the sequence of bHLH for hesC, full-length sequence for alx1, T-box sequence for tbr, C-terminal 74 amino acid sequence of the Ets domain for ets1, C-terminal 108 amino acid sequence of Gcm domain for gcm, and C-terminal 83 amino acid sequence of peptidyl-prolyl cis-trans isomerase domain for cyp1 were used. (A) Identification of *PbhesC*. The phylogenetic tree suggests the isolated gene belongs to the HES family but not the HERP family. In the echinoderm *hesC* group (green box) of the HES family, the *PbhesC* candidate is closely related to the other echinoid *hesC* genes rather than the asteroid *hesC*. (B) Identification of *Pbalx1*. The tree clearly supports that the isolated sequence is included in the Cart1 group. Cart1 genes were divided into 2 groups: genes from vertebrates and *alx* genes of echinoids. *Pbalx1* was in the group of the echinoid *alx1* genes (blue box) but not in *alx4*. (C) Identification of *Pbtbr*. Analysis using 3 subfamily genes of the T-box family (*Tbr*, *Bra*, and *Tbx*) supported the theory that the isolated gene belongs to the echinoderm *Tbr* family (green box). In echinoderm *tbr* genes, our candidate sequence was separated into echinoid *tbr* (blue box) and asteroid *tbr*. (D) Identification of *Pbgcm*. The tree shows that the *gcm* family genes were classified into genes from echinoderms (green box) and the other animals. Among echinoderm genes, the isolated gene showed a higher homology with the other echinoid *gcm* genes (blue box) than with the asteroid *gcm*. (E) Identification of *Pbcyp1*. The

phylogenetic tree analyzed with 8 *cyclophillin* genes identified in *Strongylocentrotus purpuratus* suggests that *Spcyclophilin1* shows the highest homology to the isolated gene (bootstrap support 100%). (F) Identification of *Pbets1*. The C-terminal 74 amino acid sequence of the isolated gene was compared with those of the other *ets* family genes. Our sequence is 100% identical to those deduced from echinoid *ets1* genes (*Smets1, PlETS1, and Spets1*) and is identical, except for 1 amino acid, with that of asteroid *ets1* ortholog. In contrast, there were a number of differences in the amino acid residues compared with the sequences of other *ets* family genes identified in *S. purpuratus* (*Sp-Pea, Sperg, and Sp-Gabp*). Accession numbers are as follows: Sp-HesC, SPU_021608; HphesC, AU274707; SmhesC, AB569638; PmHesC, GU251976; SpHes, AY445629; Sk-hes1, NM_001164994; Dmh, NM_001014577; Sp-Hairy, SPU_006813; Sp-Hey4, SPU_015712; DmE(spl)-HLH-mdelta, X67048; DmHesr-1, AF151523; Sp-Hey, SPU_009465; HsHEY1, NM_012258; SpAlx1, NM_214644; LvAlx1, AY277400; PlAlx1, DQ536192; Smalx1, AB569635; Sp-Alx4, SPU_22816; MmAlx1, NM_172553; Drcart1, GU056833; MmAlx3, NM_007441; MmAlx4, NM_007442; Dmal, NM_164382; Drarx, NM_131384; MmArx, NM_007492; Sp-Arx, XM_001189711; PlSKE-T, AJ309216; HpTb, EF530737; Pjtbr, FJ715949; Smtbr, FJ714958; Ap-T-brain, AB032259; Sktbr1, NM_001164990; MmEomes, NM_010136; MmTbr1, NM_009322; MmTbx6, AY654733; Sp-Tbx-2-3, SPU_023386; MmTbx2, AF244917; MmTbx1, AF349658; Sp-Bra, SPU_013015; MmT, NM_009309; Pmgcm, HP129833; LvGCM; EU306538; Spgcm; NM_214661; BfGcm; XM_002591735; Dmgcm; U34039; MmGcm2; NM_008104; MmGcm1; NM_008103; Spcyclophilin1, NM_0016033647; Sp-Ppib, SPU_013756; Sp-Pdpi (cyclophilin) L7, SPU_008305; Sp-Pdpi (cyclophilin) L5, SPU_000637; Sp-Pdpi (cyclophilin) L8, SPU_028896; Sp-Ppil4; SPU_004626; Sp-Pdpi (cyclophilin) L6, SPU_015088; Sp-Pdpi (cyclophilin) L9, 022479;

Smets1; AB569636; PlEts1; AY442298; SpEts1; NM_214533; ApEts; AB569245; Sp-Pea; SPU_014576; SpErg; AY508725; and Sp-Gapb; SPU_021557.

Fig. S2.

Spatial gene expression analysis at the mid-blastula, mid-gastrula, and pluteus stages and quantitative expression analysis through early development of the *P. baculosa* embryo. (A1–G1 and H) Mid-blastulae at 12 h postfertilization (hpf). (A2–G2) Mid-gastrulae at 25 hpf. (A3–G3) Pluteus larvae at 72 hpf. (A1–A3) Embryonic development. (A1 and A3) Living embryos. (A2) Immunohistochemistry was performed on the fixed embryo with a P4 antibody. The expression of P4 is observed in the mesenchyme cells ingressed into the blastocoel. (B1–G1, B2–G2, B3–G3, and H) The embryo analyzed by whole-mount *in situ* hybridization (WMISH). Scale bar = 50 μm. (B4–G4) Transcript levels analyzed by quantitative real-time polymerase chain reaction (QPCR) from the unfertilized egg (0 hpf) to the pluteus larva (72 hpf) stages. The X-axis shows the time after fertilization. The Y-axis shows the relative amount of subjected mRNA to *PbmitCOI* mRNA. The error bars show standard deviations. (I) Table showing the onset of *Pbalx1*, *Pbtbr*, *Pbets1*, and *Pbgcm* expression during the early embryonic stages. The number of embryos with localized gene expression was counted at 4 stages: 64-cell (6 hpf), 120-cell (8 hpf), 240-cell (10 hpf), and 420-cell (12 hpf) stages. Hpf: hours postfertilization. ND: not determined.

[Transition of mRNA expression level through early development]

For all genes other than *Pbalx1*, maternal mRNA is detected. (B4) Expression of *PbhesC* continues from the egg (0 hpf) until the pluteus larva (72 hpf) stage. (C4–F4) The expression levels of *Pbalx1*, *Pbtbr*, *Pbets1*, and *Pbgcm* increased during the blastula stages and reached a peak at the gastrula

stage (25 hpf or 36 hpf). (G4) The expression level of *Pbcyp1* markedly increased at 25 hpf and reached a peak at 36 hpf.

[The onset of region-specific expression]

Strong expression regions of *PbhesC* can be observed as spots in whole embryos by the 120-cell stage (8 hpf). (I) Localized expression of *Pbalx1* and *Pbets1* starts at the 120-cell stage (8 hpf), whereas that of *Pbtbr* and *Pbgcm* starts at the 240-cell stage (10 hpf) at 1 pole of the embryo. As mentioned below, region-specific expression of *Pbcyp1* starts from the mid-gastrula stage.

[The expression pattern at mid-blastula stage (12 hpf)]

(B1) There are a number of spots expressing *PbhesC* at this stage. To examine the relationship between the location of patches and the animal–vegetal axis, double-WMISH with the vegetal pole marker *Pbwnt8* (Yamazaki et al., 2012) was performed. In the double-stained embryos, 1 of the patches of *PbhesC* expression (arrowhead) was always observed in the center of the *Pbwnt8*-expressing area (orange double-headed arrow), suggesting that the vegetal pole cells express *PbhesC*. (C1–F1) The expression regions of *Pbalx1* (C1), *Pbtbr* (D1), *Pbets1* (E1), and *Pbgcm* (F1) are located at 1 pole of the mid-blastula. The multiplex-WMISH using RNA probes of *wnt8*, *alx1*, *tbr*, *ets1*, and *gcm* (H). All the embryos analyzed had 1 spot, which included *alx1*, *tbr*, *ets1*, and *gcm* expression, located in the center of the *wnt8*-expressing region (orange double-headed arrow in H), suggesting their vegetal expression. (G1) *Pbcyp1* does not show obvious expression.

[The expression pattern at the mid-gastrula stage (25 hpf)]

(B2–G2) The expression of all genes is observed in the archenteron (bracket) and/or the ingressed mesenchyme cells. Four genes other than *PbhesC* and *Pbgcm* are expressed in the ingressed skeletogenic mesenchyme cells. White arrowheads in (B2) and (F2) indicate mesenchyme cells with

no gene expression. In the archenteron, the lower part expresses *PbhesC* (B2), the middle part expresses *Pbgcm* (F2), and the upper regions shows expression of *Pbtbr*, *Pbets1*, and *Pbcyp1* (D2, E2, and G2).

[The expression pattern in the pluteus larva at 72 hpf]

(B3–G3) The obvious expression of all genes other than *Pbtbr* is detected at this stage. (B3) Expression of *PbhesC* is observed in the tip of the archenteron (arrow) and the coelomic pouch (arrowhead) as well as the ectodermal region. (C3) The pluteus larva weakly expresses *Pbalx1* in the mesenchyme cells positioned along the postoral rods. (E3) *Pbets1* is expressed in both the ectoderm and the mesenchyme cells located in the tip of the postoral arms (double-headed arrows). (F3) The *Pbgcm*-expressing cells are located in the tip of the archenteron, the coelomic pouches (arrowhead), or the ectoderm (arrow). (G3) Expression of *Pbcyp1* is detected in the coelomic pouches (arrows) and in mesenchyme cells at the tip of the postoral rods (arrowheads) as well as some other regions.

Fig. S3.

QPCR analysis of *hesC* mRNA in hesC perturbed embryos of *P. baculosa* (A), *S. mirabilis* (B), and *H. pulcherrimus* (C). Analyses are performed at the blastula stage. The hpf is indicated in the upper left corner of each graph. The Y-axis shows the cycle difference (Ct) in QPCR when compared with the uninjected control. The results from 2 batches are shown. Error bars are standard deviations. In all cases, the amount of *hesC* mRNA is significantly increased by species-specific hesC-MO, whereas the MO derived from the sequence of another species shows no effect.

Figure S1.

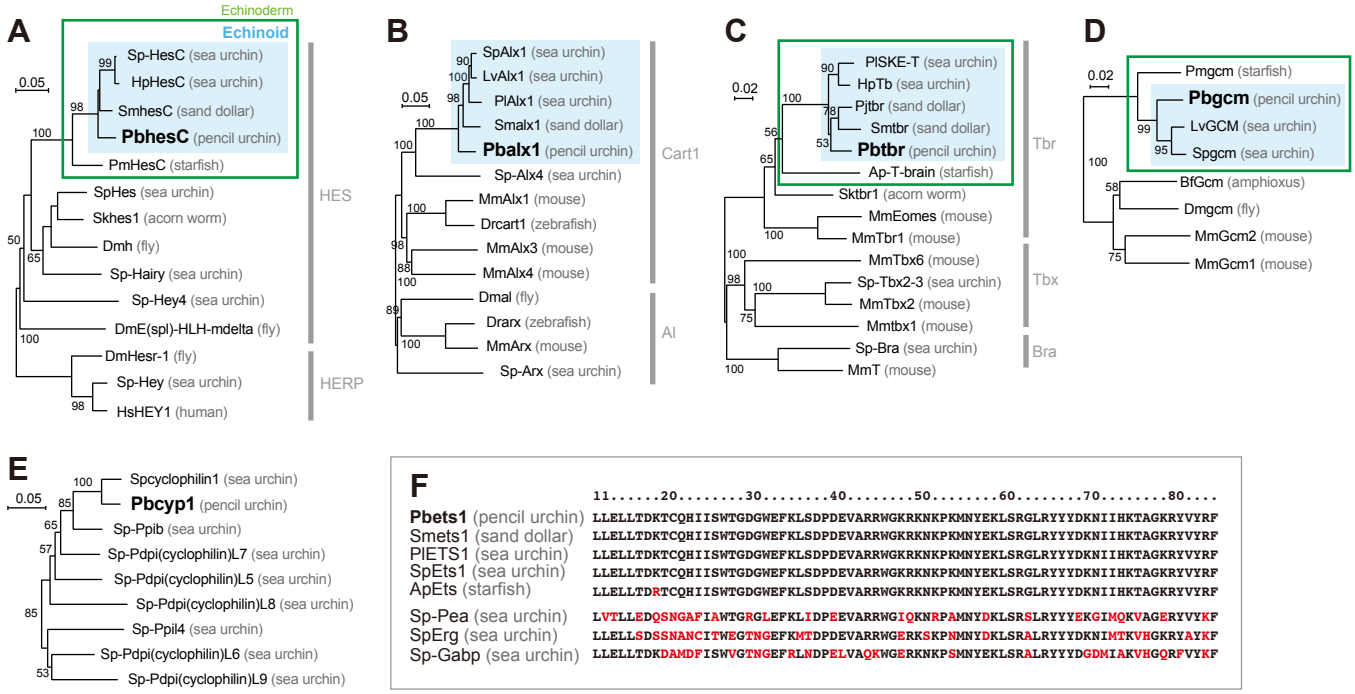
A
Echinoderm
Echinoid
Sp-HesC (sea urchin)
HpHesC (sea urchin)
SmhesC (sand dollar)
PbhesC (pencil urchin)
PmHesC (starfish)
SpHes (sea urchin)
Skhes1 (acorn worm)
Dmh (fly)
Sp-Hairy (sea urchin)
Sp-Hey4 (sea urchin)
DmE(spl)-HLH-mdelta (fly)
DmHesr-1 (fly)
Sp-Hey (sea urchin)
HsHEY1 (human)
HES
HERP
B
SpAlx1 (sea urchin)
LvAlx1 (sea urchin)
PlAlx1 (sea urchin)
Smalx1 (sand dollar)
Pbalx1 (pencil urchin)
Sp-Alx4 (sea urchin)
MmAlx1 (mouse)
Drcart1 (zebrafish)
MmAlx3 (mouse)
MmAlx4 (mouse)
Dmal (fly)
Drarx (zebrafish)
MmArx (mouse)
Sp-Arx (sea urchin)
Cart1
Al
C
PlSKE-T (sea urchin)
HpTb (sea urchin)
Pjtbr (sand dollar)
Smtbr (sand dollar)
Pbtbr (pencil urchin)
Ap-T-brain (starfish)
Sktbr1 (acorn worm)
MmEomes (mouse)
MmTbr1 (mouse)
MmTbx6 (mouse)
Sp-Tbx2-3 (sea urchin)
MmTbx2 (mouse)
Mmtbx1 (mouse)
Sp-Bra (sea urchin)
MmT (mouse)
Tbr
Tbx
Bra
D
Pmgcm (starfish)
Pbgcm (pencil urchin)
LvGCM (sea urchin)
Spgcm (sea urchin)
BfGcm (amphioxus)
Dmgcm (fly)
MmGcm2 (mouse)
MmGcm1 (mouse)
E
Spcyclophilin1 (sea urchin)
Pbcyp1 (pencil urchin)
Sp-Ppib (sea urchin)
Sp-Pdpi(cyclophilin)L7 (sea urchin)
Sp-Pdpi(cyclophilin)L5 (sea urchin)
Sp-Pdpi(cyclophilin)L8 (sea urchin)
Sp-Ppil4 (sea urchin)
Sp-Pdpi(cyclophilin)L6 (sea urchin)
Sp-Pdpi(cyclophilin)L9 (sea urchin)
F
11.....20.....30.....40.....50.....60.....70.....80....
Pbets1 (pencil urchin) LLELLTDKTCQHIISWTGDGWEFKLSDPDEVARRWGKRKNKPKMNYEKLSRGLRYYYDKNIIHKTAGKRYVYRF
Smets1 (sand dollar) LLELLTDKTCQHIISWTGDGWEFKLSDPDEVARRWGKRKNKPKMNYEKLSRGLRYYYDKNIIHKTAGKRYVYRF
PlETS1 (sea urchin) LLELLTDKTCQHIISWTGDGWEFKLSDPDEVARRWGKRKNKPKMNYEKLSRGLRYYYDKNIIHKTAGKRYVYRF
SpEts1 (sea urchin) LLELLTDKTCQHIISWTGDGWEFKLSDPDEVARRWGKRKNKPKMNYEKLSRGLRYYYDKNIIHKTAGKRYVYRF
ApEts (starfish) LLELLTDRTCQHIISWTGDGWEFKLSDPDEVARRWGKRKNKPKMNYEKLSRGLRYYYDKNIIHKTAGKRYVYRF
Sp-Pea (sea urchin) LVTLLEDQSNGAFIAWTGRGLEFKLIDPEEVARRWGIQKNRPAMNYDKLSRSLRYYYEKGIMQKVAGERVVYKF
SpErg (sea urchin) LLELLSDSSNANCITWEGTNGEFKMTDPDEVARRWGERKSKPNMNYDKLSRALRYYYDKNIMTKVHGKRYAYKF
Sp-Gabp (sea urchin) LLELLTDKDAMDFISWVGTNGEFRLNDPELVAQKWGERKNKPSMNYEKLSRALRYYYDGDMIAKVHGQRFVYKF

Figure S2.

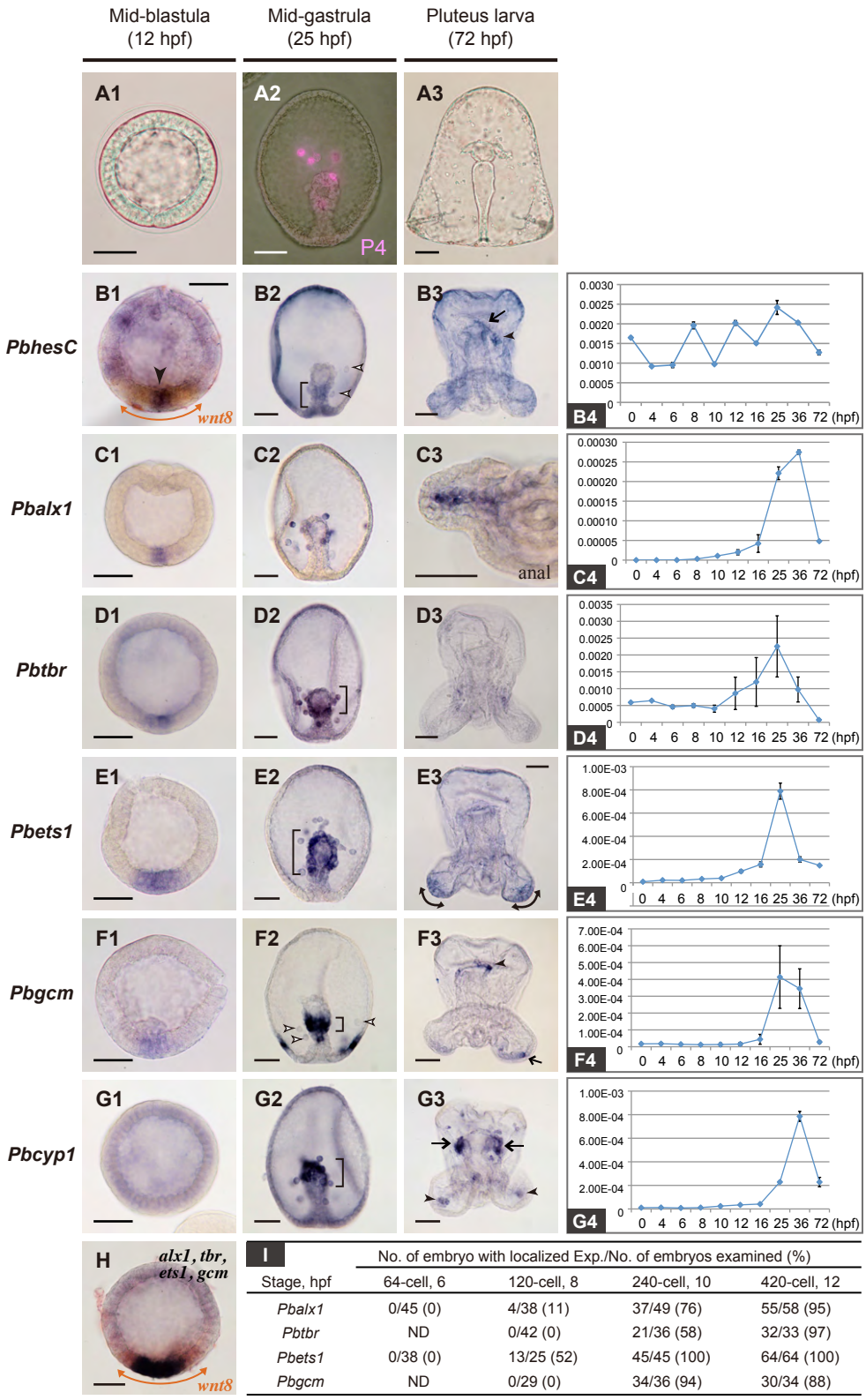

I

Stage, hpf	No. of embryo with localized Exp./No. of embryos examined (%)			
	64-cell, 6	120-cell, 8	240-cell, 10	420-cell, 12
Pbalx1	0/45 (0)	4/38 (11)	37/49 (76)	55/58 (95)
Pbtbr	ND	0/42 (0)	21/36 (58)	32/33 (97)
Pbets1	0/38 (0)	13/25 (52)	45/45 (100)	64/64 (100)
Pbgcm	ND	0/29 (0)	34/36 (94)	30/34 (88)

Figure S3.

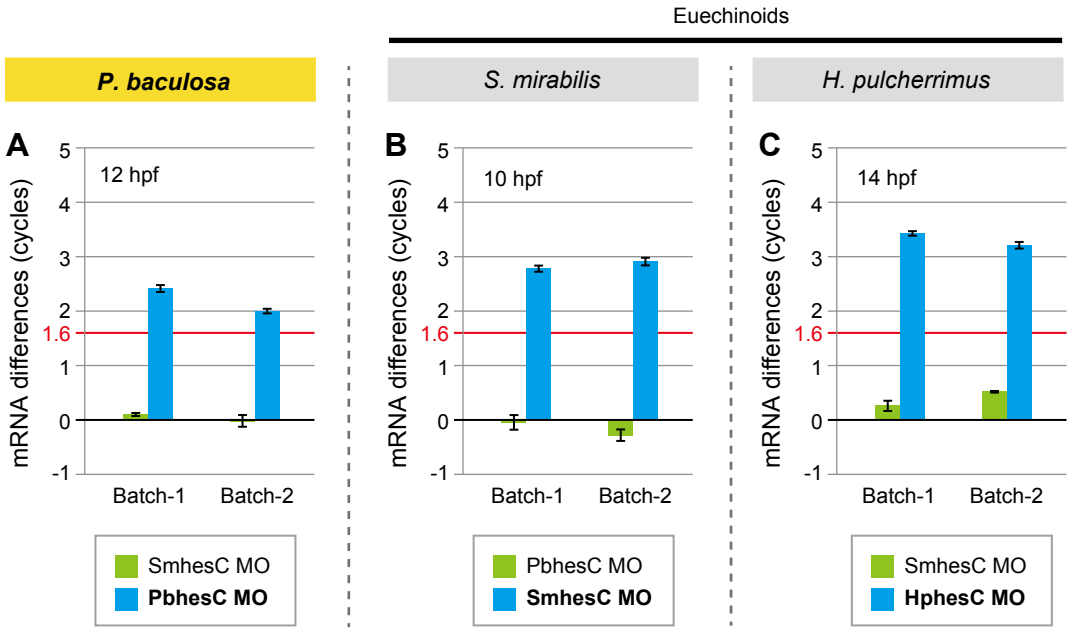
Euechinoids
P. baculosa
S. mirabilis
H. pulcherrimus
A
B
C
12 hpf
10 hpf
14 hpf
mRNA differences (cycles)
5
4
3
2
1.6
1
0
-1
Batch-1
Batch-2
SmhesC MO
PbhesC MO
PbhesC MO
SmhesC MO
SmhesC MO
HphesC MO

Table S1. Transition of total cell numbers during early development

Hpf	5	6	8	10	12	16
Average ±	31.8 ±	61.5 ±	128.9 ±	246.4 ±	449.8 ±	556.6 ±
SD	1.8	1.5	28	46	49	56
Range	30–32	61–62	120–147	232–272	423–470	495–624

Hpf: hours postfertilization.

Average: the average of total cell numbers from 10 individuals.

SD: standard deviation.

Range: from the minimum number to the maximum number.

Table S2. Primers used in the present study.

Gene	Utilize	Primer name	Sequence 5′–3′
PbhesC	degenerate PCR	F	AARATGGARAARGCTGAYAT
		R	HGCANCGRTCNGCNAGRTG
	RACE	F1	GACAGTGCGTTACTTGAAAGAGCTCCAG
		F2	AGTCGAGTGAGGGCAGCAGACCGTTGT
		R1	TGTCGAGGTCGATACTCTCGCAGGATGA
		R2	GCTGGAGACCTCACTCAAACATTCGGTGAAG
	QPCR	F	CACATGCAGTCCAGGCAGTT
		R	GCCTGGCGAGGAAAGACTAA
Pbalx1	degenerate PCR	F	AAARMGNMGNAAYMGNACNACNTT
		R	ATANCCRTTCATCATNCCNAYNAC
	RACE	F1	CACGAGTTATCAGCTGGAGGAAATGGAGAAG
		F2	TCCAGACGTATATTGCAGAGAACAACTC
		R1	TGGCCTCTGTTAGGTCACATCTGAGAGC
		R2	GAGTTGTTCTCTGCAATATACGTCTGGAT
	QPCR	F	GTGAGCGGTTCCAGCAGTTT
		R	CTGGTGGTTGATGCGTGTCT
Pbtbr	RACE	F1	CGCTCCAGTACAACGTGTTTGTCGATATG
		F2	GGTCCCATGTGGCCAGGCTGAGAAT
		R1	CTGCGTCTCGGGAAAGCTATGGGTCTGAA
		R2	CTAACACATGGATGCGAGGTTGGTACTTG
	QPCR	F	CAATCATCGAGGGAAGGACAA
		R	GGATTCTTCGGTCGCTCAGT
Pbets1	RACE	F1	ACATGTCAGCACATCATCAGCTGGACC
		F2	AGTTCAAGCTCTCCGACCCGGACGAA
	QPCR	F	GGCAAGCGCAAGAACAAAC
		R	CTGGAGATCGCACACGAATC
Pbgcm	degenerate PCR	F	GGGNTGGGCNATGMGNAAYAC
		R	CCARAARTGNGTNACNGGRTA
	RACE	F1	AGGTGTTTTCGTTTGCTCCAACAACTGTCA

		F2	ACATTGTCACCGTTCGACCGGCCACGT
	QPCR	F	ACGCTTCAAGCCAAGACGAT
		R	TGCCGAAGGAAGCATAACTG
Pbcyp1	degenerate PCR	F	CAARTTYCAYMGNGTNAT
		R	CTTNCCRWANACNACRTG
	RACE	F1	GATTCAAGGCGGTGACTTTGTCTCAGTAG
		F2	GAGGATGAGAACTTCAAGCTGGACCACTA
	QPCR	F	CCAACGGTTGCCAGTTCTAC
		F	TTCAATGGCCTTCACCACAT
PbmitCO1	QPCR	F	CGGAATGGTTTATGCGATGA
		R	TCCGGTTGGAACTGCTATGA
SmmitCO1	QPCR	F	TTCCTAGTTTGAGCCCACCAT
		R	AGTGGGAACGGCGATTATCA
SmhesC	QPCR	F	ATGACGGTGCGTTACCTGAA
		R	TTCTCGCACGATGACATGAA
HpmitCO1	QPCR	F	CCGCATTCTTGCTCCTTCTT
		R	TGCTGGGTCGAAGAAAGTTG
HphesC	QPCR	F	TGTGCCATCACCAGTCACAG
		R	GTGTTGGCTGGAAGGAGGAG